An embedded cohesive crack model for finite element analysis of concrete fracture

José M. Sancho, Jaime Planas & David A. Cendón
Universidad Politécnica de Madrid, Madrid, Spain.

ABSTRACT: This paper presents a numerical implementation of cohesive crack model for the analysis of concrete fracture based on the strong discontinuity approach. A simple central force model is used for the stress vs. crack opening law. The only material data required are the elastic constants and the mode I softening curve. The additional degrees of freedom defining the crack opening are determined at the crack level, thus avoiding the need of performing a static condensation at the element level. The need for a tracking algorithm is avoided using a consistent procedure for the selection of the separated nodes. Numerical simulations of well known experiments are presented to show the ability of the proposed model to simulate fracture of concrete.

Keywords: concrete fracture, finite element, embedded crack, localization.

1 INTRODUCTION

Considerable effort has been applied to develop robust numerical algorithms to describe tensile fracture in concrete and other quasibrittle materials.

The elder approaches to the finite element modeling of fracture, the smeared crack and the discrete crack, have been in the past years successfully complemented by the application of the so-called strong discontinuity approach (SDA) (Simo et al. 1993) . In contrast to the smeared crack model, in the SDA the fracture zone is represented as a discontinuous displacement surface. In contrast to the discrete crack approach, in the SDA the crack geometry is not restricted to inter-element lines, as the displacement jumps are embedded in the corresponding finite element displacement field.

For a comparative study of the various approaches to the embedded crack concept proposed in the literature the reader is addressed to Jirásek (2000).

Embedding discontinuous displacements in the element formulation is not the only way to implement the SDA in the finite element method. Recently the so called extended finite element method, based on nodal enrichment and the partition of unity concept, have opened a very fruitful way to the modeling of fracture.

However, extended finite elements require a greater implementation effort as compared to elements with embedded discontinuities. The advantages and disadvantages of both strategies can be found in Jirásek & Belytschko (2002) and in Wells (2001).

The objective of this paper is to show how, by means of simple considerations, using finite elements with embedded cohesive crack still remains an efficient option to model concrete fracture.

A consistent derivation of finite element with embedded discontinuities can be done in the frame of the enhanced assumed strain method (EAS) proposed by Simo & Rifai (1990). The strain induced for the displacement jumps are then tackled as additional incompatible modes. A problem of this approach is that, as the additional modes are determined at the element level, the progress of the crack may lock because of kinematical incompatibility between the cracks in neighboring elements.

One solution to avoid this problem is to use an algorithm to reestablish the geometric continuity of the crack line across the elements, a procedure known as crack tracking (Oliver et al. 2002). Most practical implementations use tracking to avoid crack locking. Moreover, some implementations further require establishing exclusion zones defined to avoid the formation of new cracks in the neighborhood of existing cracks.

This kind of algorithms constitute an inconvenient to the implementation of the embedded crack elements in standard finite

element programs, and is therefore of the greater interest to develop a method that circumvents the need of the crack path enforcement.

The SDA provides a consistent framework to transform a weak discontinuity in which the displacement is continuous but the strain is discontinuous at the boundaries of a band of a certain width h, into a strong discontinuity in which the displacement is discontinuous at a surface. Thus, the strong discontinuity (displacement jump) is obtained as the limit of a weak discontinuity band when the bandwidth h tends to zero. In this way the discrete constitutive model for the discontinuity naturally arises induced by the continuum model. This is an elegant and sound standpoint for the study of shear bands in soils and metals. However in the fracture of concrete, it is simpler and more effective to use a discrete constitutive model that relates the tractions and displacement jumps at the discontinuity line. This approach is used in the present work.

2 A SIMPLE COHESIVE CRACK MODEL

Previous works (Cendón et al. 2000, Gálvez et al. 2002) showed that for most experiments described in the literature, cohesive crack growth takes place under predominantly local mode I, which implies that the overall behavior is dominated by mode I parameters. In consequence, in this work, a simple generalization of the cohesive crack to mixed mode is used which assumes that the traction vector **t** transmitted across the crack faces is parallel to crack displacement vector **w** (central forces model). It is further assumed that the cohesive crack unloads to the origin (Figure 1) and write the equation as:

$$\mathbf{t} = \frac{f(\tilde{w})}{\tilde{w}}\mathbf{w} \qquad \text{with } \tilde{w} = \max(|\mathbf{w}|) \tag{1}$$

where $f(\tilde{w})$ is the classical softening function for pure opening mode, and $\tilde{w}$ is an equivalent crack opening defined as the historical maximum of the norm of the crack displacement vector.

3 FINITE ELEMENT MODELLING

The basic aim of the modeling is to be able to describe concrete cracking in 2D. The crack is numerically implemented as a discontinuity embedded in a classical finite element.

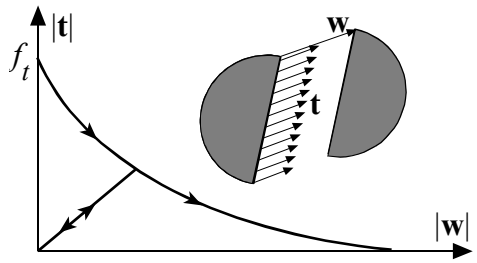

Figure 1: Sketch of the softening curve for the cohesive crack model.

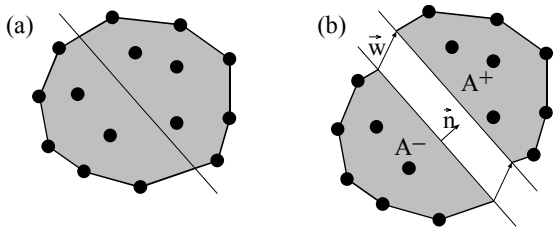

Figure 2: Finite element with a crack with uniform opening: (a) generic element with nodes and crack line; (b) displacement jump across the crack line.

3.1 *Finite element formulation*

Consider an arbitrary classical finite element defined by a node layout as shown in Figure 2a. Assume that a straight crack is embedded in it. Take one of the faces of the crack as the reference, the normal **n** to it as the positive normal. Let **w** be the displacement jump across the crack of the opposite side of the crack with respect to the reference side (see Figure 2b). The crack splits the element in two sub-domains A^+ and A^-. Following the strong discontinuity approach (e.g., Oliver 1996), the approximated displacement field within the element can be written as:

$$\mathbf{u}(\mathbf{x}) = \sum_{\alpha \in A} N_\alpha(\mathbf{x})\mathbf{u}_\alpha + \left[H(\mathbf{x}) - N^+(\mathbf{x})\right]\mathbf{w} \tag{2}$$

where α is the element node index, $N_\alpha(\mathbf{x})$ the traditional shape function for node α, $\mathbf{u}_\alpha$ the corresponding nodal displacement, $H(\mathbf{x})$ the Heaviside jump function across the crack plane [i.e., $H(\mathbf{x})=0$ for $\mathbf{x}\in A^-$, $H(\mathbf{x})=1$ for $\mathbf{x}\in A^+$], and $N^+(\mathbf{x})=\Sigma_{\alpha\in A^+} N_\alpha(\mathbf{x})$.

The strain tensor is obtained from the displacement field as a continuous part $\boldsymbol{\varepsilon}^c$ plus a Dirac's δ function on the crack line. The continuous part, which determines the stress field on the element on both sides of the crack, is given by

$$\boldsymbol{\varepsilon}^c(\mathbf{x}) = \boldsymbol{\varepsilon}^a(\mathbf{x}) - \left[\mathbf{b}^+(\mathbf{x}) \otimes \mathbf{w}\right]^S \tag{3}$$

where $\boldsymbol{\varepsilon}^a$ and $\mathbf{b}^+$ are given by

$$\boldsymbol{\varepsilon}^a(\mathbf{x}) = \sum_{\alpha \in A} \left[\mathbf{b}_\alpha(\mathbf{x}) \otimes \mathbf{u}_\alpha \right]^S \tag{4}$$

$$\mathbf{b}^+(\mathbf{x}) = \sum_{\alpha \in A^+} \mathbf{b}_\alpha(\mathbf{x}) \tag{5}$$

with $\mathbf{b}_\alpha(\mathbf{x})=\text{grad}N_\alpha(\mathbf{x})$ and superscript ^{S} indicating symmetric part of a tensor. Obviously, $\boldsymbol{\varepsilon}^a$ is the *apparent* strain tensor of the element computed from the nodal displacements.

3.2 *Crack tractions*

Along the cohesive crack line, the jump vector **w** and the traction vector **t** are to be related by Equation 1. For the exact solution, the traction vector is computed locally as $\mathbf{t}=\boldsymbol{\sigma}\mathbf{n}$. For the finite element, however, we must deal with approximate tractions and crack jump vectors, and there is not a single way to determine the relationship between the approximate stress field and the tractions. To simplify the reasoning, we approximate the traction field along the crack line by a constant traction $\bar{\mathbf{t}}$. The determination of $\bar{\mathbf{t}}$ is approximate, and can be done in two different ways: 1) as an average along the crack line of the local traction vector $\boldsymbol{\sigma}\mathbf{n}$, or (2) by forcing the global equilibrium of either A^+ or A^- (which is equivalent, in this case, to using the principle of virtual work). The corresponding equations read:

$$\bar{\mathbf{t}} = \frac{1}{L} \int_L \boldsymbol{\sigma}\mathbf{n}\, dl \tag{6}$$

$$\bar{\mathbf{t}} = \frac{1}{L} \int_A \boldsymbol{\sigma}\mathbf{b}^+ dA \tag{7}$$

in which the stress tensor is that corresponding to the classical FE approximation based on the continuous strain in Equation 3. In general, the two equations do not coincide, as shown next for constant strain triangles with an embedded crack.

3.3 *Constant strain triangle*

Consider a constant strain triangle with a strong discontinuity line (crack) such as shown in Figure 3a, and select the positive normal pointing towards the solitary node. Then it is easy to show that

$$\mathbf{b}^+ = \frac{1}{h} \mathbf{n}^+ \tag{8}$$

where h is the height of the triangle over the side opposite to the solitary node and $\mathbf{n}^+$ the unit normal to that side. With this, and the fact that the stresses are uniform, Equations 6 and 7 reduce to

$$\bar{\mathbf{t}} = \boldsymbol{\sigma}\mathbf{n} \qquad \text{for local equilibrium} \tag{9}$$

$$\bar{\mathbf{t}} = \frac{A}{hL} \boldsymbol{\sigma}\mathbf{n}^+ \qquad \text{for global equilibrium} \tag{10}$$

where A is the area of the element and L the length of the crack. This shows that for local and global equilibrium to hold, it is required that $\mathbf{n}^+ = \mathbf{n}$ and $hL = A$. This reduces to the following two conditions: (1) the discontinuity (crack) line must be parallel to one of the sides of the triangle, and (2) the discontinuity line must be located at mid height. Thus the potential crack lines satisfying both local and global equilibrium are those indicated by dashed lines in Figure 3b.

In our approach the local equilibrium Equation 9 is used in conjunction with the strain approximant Equation 3. This leads to a nonsymmetric formulation (SKON, according to the nomenclature in Jirásek 2000). If Equation 10 is used then a symmetric formulation is obtained (Jirásek's KOS formulations). Note, however, that both formulations tend to coincide when the crack runs parallel to one side of the element and at mid height (*not* through the centroid).

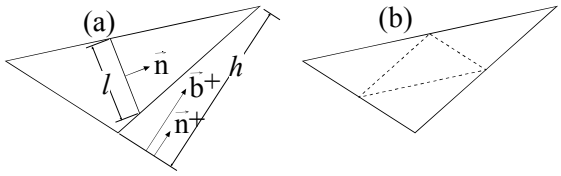

Figure 3: Constant stress triangle: (a) geometrical definitions; (b) potential crack path satisfying both local and global equilibrium (dashed lines)

4 NUMERICAL IMPLEMENTATION

The implementation assumes linear elastic behavior of the material outside the crack. The crack displacement vector **w** is handled as two internal degrees of freedom which are solved at the level of the crack within the element.

4.1 *Basic equations*

One of the main tasks of the implementation is to compute the stress tensor in the element, which follows an algorithm similar to plasticity, since the stress tensor is given, from Equation 3 and the hypothesis of elastic bulk material behavior, as

$$\boldsymbol{\sigma} = \mathbf{E}\left[\boldsymbol{\varepsilon}^a - \left(\mathbf{b}^+ \otimes \mathbf{w} \right)^S \right] \tag{11}$$

where $\boldsymbol{E}$ is the tensor of elastic moduli. Before computing the result for the stress, the crack displacement must be solved for, which is done from Equation 9 and the cohesive crack Equation 1, which lead to the condition

$$\frac{f(\tilde{w})}{\tilde{w}}\mathbf{w} = \left[\mathbf{E}\boldsymbol{\varepsilon}^a\right]\mathbf{n} - \mathbf{E}\left[\boldsymbol{\varepsilon}^a - \left(\mathbf{b}^+ \otimes \mathbf{w}\right)^S\right]\mathbf{n} \qquad (12)$$

This equation is solved for $\mathbf{w}$ using Newton-Raphson's method given the nodal displacements (and so $\boldsymbol{\varepsilon}^a$) once the crack is formed and thus $\mathbf{n}$ and $\mathbf{b}^+$ are also given. One of the key points in the proposed method is how the crack is introduced in the element, i.e., how $\mathbf{n}$ and $\mathbf{b}^+$ are determined.

4.2 *Crack initiation*

Initially, $\mathbf{w} = \mathbf{0}$ in the element, and $\mathbf{n}$ and $\mathbf{b}^+$ are undefined. Thus, the element loads elastically and $\boldsymbol{\sigma} = \mathbf{E}\boldsymbol{\varepsilon}^a$ until the maximum principal stress exceeds the tensile strength. Then a crack is introduced perpendicular to the direction of the maximum principal stress, and $\mathbf{n}$ is computed as a unit eigenvector of $\boldsymbol{\sigma}$.

Next, the solitary node and the vector $\mathbf{b}^+$ are determined by requiring that the angle between $\mathbf{n}$ and $\mathbf{b}^+$ be the smallest possible (see Figure 3). This is equivalent to selecting the solitary node so that the side opposite to it be as parallel as possible to the crack. This procedure was devised based on the observation of Borja (2000) that the behavior of this type of element is best when the crack meets such condition, and also based on the analysis in the previous section showing that the local and global equilibrium are simultaneously met only when $\mathbf{n}$ is parallel to $\mathbf{b}^+$.

4.3 *Crack adaptation*

The foregoing procedure is done at the element level, and is strictly local: no crack continuity is enforced or crack exclusion zone defined. This leads in many circumstances to locking after a certain crack growth. Such locking seems to be due to a bad prediction of the cracking direction in the element ahead of the pre-existing crack, as sketched in Figure 4.

To overcome this problem without introducing global algorithms (crack tracing and exclusion zones), we just introduce a certain amount of crack adaptability within each element. The rationale behind the method is that the estimation of the principal directions in a triangular element is specially bad at crack initiation due to the high stress gradients in the crack tip zone where the new cracked element is usually located; after the crack grows further, the estimation of the principal stress directions usually improves substantially. Therefore we allow the crack to adapt itself to the later variations in principal stress direction *while its opening is small*.

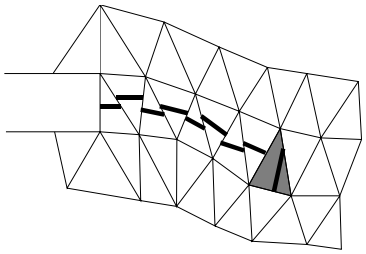

Figure 4: Sketch of crack locking: the prediction of cracking direction in the shaded element is wrong.

This crack adaptation is implemented very easily by stating that while the equivalent crack opening at any particular element $\tilde{w}$ is less than a threshold value $\tilde{w}_{th}$, the crack direction is recomputed at each step as if the crack were freshly created. After $\tilde{w} > \tilde{w}_{th}$, no further adaptation is allowed and the crack direction becomes fixed. Threshold values must be related to the softening properties of the material, and values of the order of $0.1 G_F/f_t$ are usually satisfactory. Here, G_F is the fracture energy and f_t the tensile strength.

This simple expedient has proved to be extremely effective as shown in the examples presented next, and bears some resemblance with other approaches used to avoid crack locking. For example, Tano et al (1988) used a rotating crack model to avoid locking and Jirásek and Zimmermann (2001) in which a smeared rotating crack model was introduced at the beginning of cracking. In our approach the crack adaptation is introduced to circumvent the numerical deficiency in predicting accurately the principal stress directions, and has not to be taken as a material property.

5 NUMERICAL EXPERIMENTS

5.1 *Programs used*

The model described in the preceding section has been introduced in two finite element programs: FEAP and ABAQUS.

In FEAP the model has been implemented as a user element subroutine (Taylor 2003).

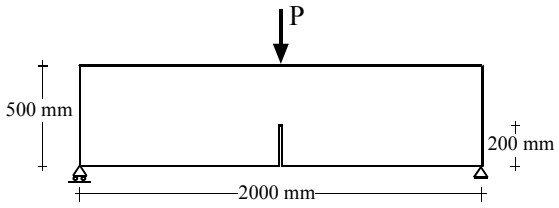

Figure 5: Three point bending test.

In ABAQUS, the model has been introduced as a user material model using the subroutine UMAT. An auxiliary external file containing the nodal coordinates and mesh element connectivity is also used. This is necessary to compute the vector $\mathbf{b}^+$ as explained in section 4.2. This file would not be needed if the model were implemented as a user element in a UEL subroutine.

As a reference, the program Splitting-Lab, based on a highly accurate boundary integral approach (smeared tip method; see Bazant & Planas 1998), was used to compute the results for the bending beam.

5.2 *Experiments*

In this section the results obtained for two different bending tests are presented.

In both examples a quasi-static analysis is performed. ,and an exponential softening curve is adopted, both for simplicity and due to a lack of direct experimental information. With this, the relationship between the normal and shear components of strain and crack opening are obtained from equation (1) as

$$t_n = f_t \frac{w_n}{\tilde{w}} \exp\left(-\frac{\tilde{w} f_t}{G_F}\right) \tag{13}$$

$$t_t = f_t \frac{w_t}{\tilde{w}} \exp\left(-\frac{\tilde{w} f_t}{G_F}\right) \tag{14}$$

where t_n and t_t are the normal and shear tractions, respectively, w_n the crack opening displacement and w_t the crack sliding displacement; G_F is the fracture energy, f_t the tensile strength and $\tilde{w}$ is obtained as

$$\tilde{w} = \max \sqrt{\left(w_n^2 + w_t^2\right)} \tag{15}$$

5.2.1 *Three point bending test*

The three point bending beam test was analyzed using different meshes. Two aspects are of interest: first to check the ability of the proposed model to trace a straight vertical crack without crack tracking, even in an unstructured mesh; second, to check whether or not the computations depend spuriously on the mesh size.

The beam dimensions were: length = 2000 mm, thickness = 100 mm, and depth = 500 mm. A single notch 200 mm in depth and 5 mm in width is introduced as shown in Figure 5.

The material parameters were taken to be as follows: tensile strength f_t = 2.5 MPa, Young modulus E= 20 GPa, Poisson's ratio ν = 0.15 fracture energy G_F = 0.1 N/mm.

The computations were run under control of the displacement at the upper midpoint.

Three different meshes were used as shown in Figure 6:

a. Fine, structured, 3664 elements
b. Coarse, structured, 1110 elements
c. Coarse unstructured, 1166 elements.

As can bee seen in the figure, the external zones of the mesh have been kept the same, and the deformed meshes at the end of the loading (1 mm deflection) look quasi identical. Note that in the structured meshes one of the side of the elements cracked is parallel to the vertical crack, so the vectors $\mathbf{n}$ and $\mathbf{b}^+$ have the same direction, and thus the crack propagates perfectly vertical.

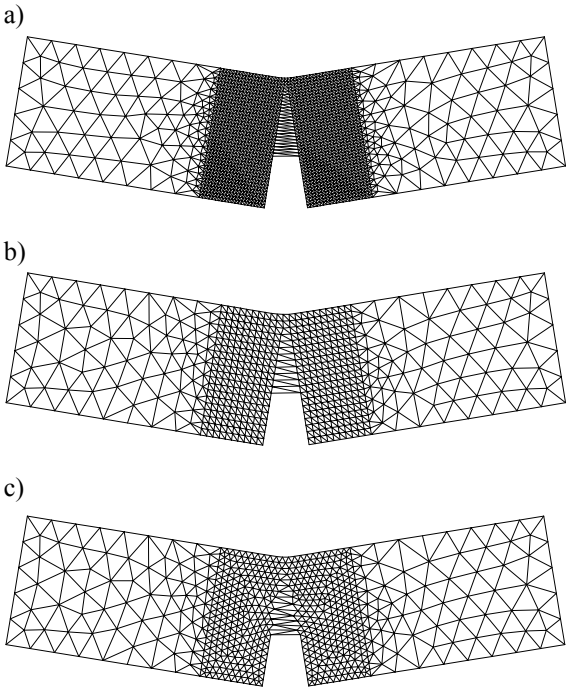

Figure 6: Deformed meshes of: a) fine structured mesh; b) coarse structured mesh; c) coarse unstructured mesh.

Figure 7 shows the load-displacement curves computed using the three meshes and a reference curve computed using the smeared tip superposition method. The agreement of all the curves is excellent: the coarse unstructured mesh slightly overestimates the peak load, and the coarse structured mesh strengthens the tail. The coarse unstructured mesh follows the tail with surprising accuracy. There is no trace of spurious mesh sensitivity.

As shown in Figure 8, the result obtained with the unstructured mesh is an excellent proof of the ability of the proposed model to trace the correct direction of the crack across elements with the sides not aligned along the macroscopic crack direction even in a so coarse mesh. The crack is therefore able to propagate independently of the mesh alignment and again the predicted load-displacement curve is essentially correct.

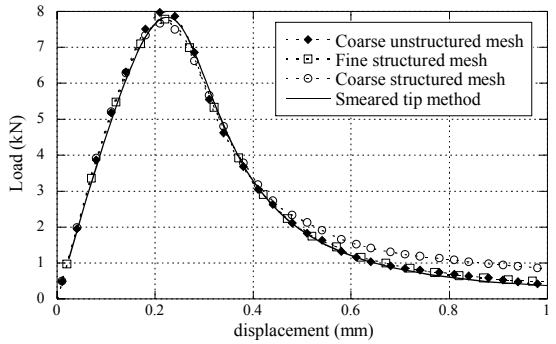

Figure 7: Numerical results for the TPB test with the three different meshes used.

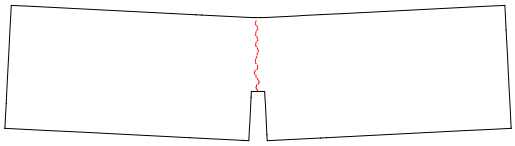

Figure 8: Crack path for the coarse unstructured mesh.

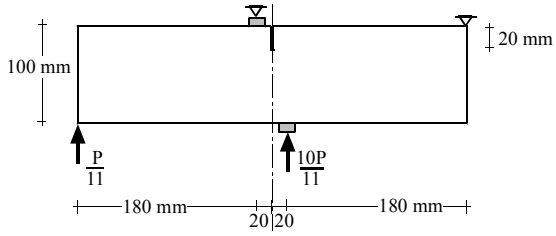

Figure 9: Single notched beam subjected to shear.

5.2.2 *Shear test beam*

The second test analyzed here corresponds to a single edge notched beam subjected to four-point shear as shown in Figure 9.

A series of tests on this type of beam were reported by Schlangen (1993) and Schlangen & van Mier (1993). Various authors have used this beam as a benchmark for numerical models. It was observed experimentally that a crack appears at the right side of the notch propagating downwards to the right support in a curved pattern.

An analysis of this test using embedded crack elements with enforced crack path continuity can be found in Alfaiate et al. (2002). For simulations using the partition of unity formulation, the reader is addressed to the work of Wells (2001).

Similar analyses were performed by Rots (1988) using the smeared crack approach which put into evidence the difficulties in correctly representing the curved geometry of the crack.

The material properties adopted in our simulation were based on the values used by other authors (e.g., Alfaiate et al. 2002): Young modulus $E = 35$ GPa, Poisson's ratio $\nu = 0.15$, tensile strength $f_t = 2.8$ MPa, and fracture energy $G_F = 0.1$ N/mm.

An indirect displacement control procedure was used and the crack mouth opening and sliding displacements (CMOD, and CMSD respectively) were recorded.

The results for a coarse mesh with 461 elements, as shown in Figure 10, are presented.

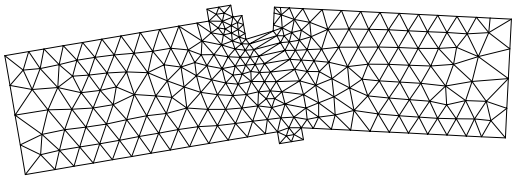

Figure 10: Deformed mesh for the single notched beam subjected to four-point shear.

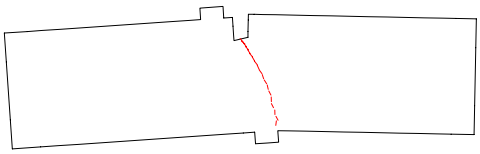

Figure 11: Crack path for the single notched beam subjected to shear.

As shown in Figure 11, the model is able to reproduce the curved character of the crack in excellent agreement with the experimental results.

Figure 12 shows the load versus CMOD and CMSD compared with the quantities measured by Schlangen. No locking occurs, and the peak load and initial part of the curve are correctly predicted by the model. The prediction of the tail could be improved by selecting a softening curve with a steeper initial descent and a stronger tail.

6 CONCLUSIONS

In this paper embedded strong discontinuities are used to model concrete fracture. The strong discontinuity is not approximated as the limit case of a weak discontinuity. Instead, the deformation is localized on a line using the concept of the cohesive crack. A discrete constitutive relation is adopted by means of a generalization of the cohesive crack to mixed mode.

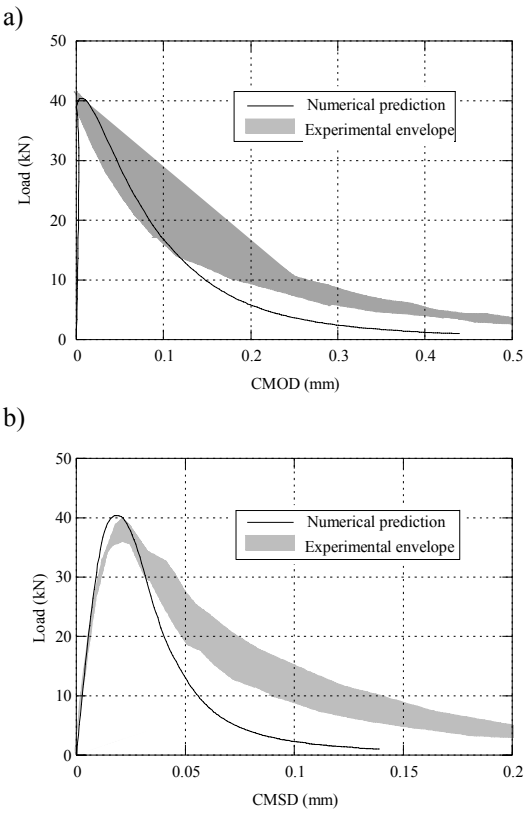

Figure 12: Numerical results for Schlangen's test; a) Load versus CMOD; b) Load versus CMSD.

A triangular constant strain finite element is formulated and implemented in standard codes. The algorithm used to obtain the crack displacement vector can be formulated at the crack level and therefore the static condensation of the stiffness matrix at the element level is avoided. The choice of the solitary node is done in a way that leads to the automatic propagation of the crack without tracking algorithm or exclusion zones. The stress locking effects are solved by letting the embedded crack in the finite element to adapt itself to the stress field while the crack opening does not exceed a small threshold value.

Finally numerical simulations of relevant tests are presented showing that the embedded crack approach is yet an effective and simpler alternative to other more sophisticated methods for the simulation of the concrete fracture.

7 ACKNOWLEDGMENTS

Thanks are given to Prof J. Oliver for his advise and fruitful discussions. The authors gratefully acknowledge financial support from the Spanish Ministerio de Ciencia y Tecnología under grant MAT2001-3863-C03-01.

8 REFERENCES

Alfaiate, J., Wells, G. N. and Sluys, L. J. 2002. On the use of embedded discontinuity elements with path continuity for mode-I and mixed-mode fracture. *Engineering Fracture Mechanics* 69(6), 661-686.

Bazant, Z.P. & Planas, J. 1998 *Fracture and Size Effect of Concrete and Other Quasibrittle Materials*. CRC Press, Boca Raton, FL, USA.

Borja RI. 2000. A finite element model for strain localization analysis of strongly discontinuous fields based on standard Galerkin approximation. *Computer Methods in Applied Mechanics and Engineering.* 190:1529-1249.

Cendón, D.A., Galvez J.C. Elices, M. & Planas J. 2000. Modelling the fracture of concrete under mixed loading. *International Journal of Fracture. Volume 103 293-310.*

Galvez, J.C. Cendón, D.A. & Planas J. 2002. Influence of shear parameters on mixed-mode fracture of concrete. *International Journal of Fracture. Volume 118 issue 22:163-189.*

Hillerborg A., Modeer M. & Petersson, P. 1976. Analysis of crack formation and crack growth in concrete by means of fracture mechanics and finite elements. *Cement and Concrete Research* 6: 773-82.

Jirásek M., 2000. Comparative study on finite elements with embedded cracks. *Computer Methods in Applied Mechanics and Engineering* 188: 307-330.

Jirásek M.,& Zimmermann T. 2001. Embedded crack model. Part II: Combination with smeared cracks. *International Journal for Numerical Methods in Engineering* 50: 1291-1305.

Jirásek M., & Belytschko T. 2002. *Fifth World Congress on Computational Mechanics*. Eds. Mang, Rammeerstorfer & Eberhardsteiner Vienna Austria .

Oliver J. 1996. Modelling strong discontinuities in solid mechanics via strain softening constitutive equations. Part 1: fundamentals. Part 2: numerical simulations. *International Journal for Numerical Methods in Engineering* 39: 3575-3623.

Oliver J. , Huespe, A. E., Samaniego, E. & Chaves, E.W.V. 2002. On strategies for tracking strong discontinuities in computational failure mechanics. *Fifth World Congress on Computational Mechanics*, Vienna, Austria.

Rots, J. 1988 . Computational Modelling of Concrete Fracture, Ph D. Thesis, Delft University of Technology.

Simo JC. & Rifai S. 1990. A class mixed assumed strain methods and the method of incompatible modes. *International Journal for Numerical Methods in Engineering* 29: 1595-1638.

Simo J., Oliver J., & Armero F. 1993. An Análisis of strong discontinuities induced by strain softening in rate-independent inelastic solids. *Computational Mechanics* 12: 277-296

Schlangen E. 1993. Experimental and numerical analysis of fracture processes in concrete. Ph D. Thesis Delft University of Technology.

Schlangen E. & van Mier J.G. 1993. Mixed-mode fracture propagation: a combined numerical and experimental study. *Fracture and damage of concrete and rock*: 166-175.

Taylor R.L. 2001. FEAP A finite Element Analysis Program. Programmer Manual. Berkeley California.

Tano R., Klisinski M., & Olofsson T. 1998. Stress locking in the inner softening band method : A study of the origin and how to reduce the effects. *Computational Modelling of Concrete Structures, De Borst, Bicanic, Mang & Meschke (eds)* Balkema, Rotterdam.

Wells G.N. 2001. Discontinuous modeling of strain localization and failure. Ph D. Thesis Delft University of Technology.